Journal of Hydrology 580 (2020) 124370

Contents lists available at ScienceDirect

Journal of Hydrology

journal homepage: www.elsevier.com/locate/jhydrol

Research papers

Mechanisms of surface and subsurface runoff generation in subtropical soil-epikarst systems: Implications of rainfall simulation experiments on karst slope

Sheng Wang[a,b,c], Zhiyong Fu[a,c,*], Hongsong Chen[a,c,*], Yunpeng Nie[a,c], Qinxue Xu[a,c]

[a] Key Laboratory of Agro-ecological Processes in Subtropical Region, Institute of Subtropical Agriculture, Chinese Academy of Sciences, Changsha, Hunan 410125, China
[b] Key laboratory of Environment Change and Resources Use in Beibu Gulf, (Nanning Normal University), Ministry of Education, Nanning, Guangxi 530001, China
[c] Huanjiang Observation and Research Station for Karst Ecosystems, Chinese Academy of Sciences, Huanjiang, Guangxi 547100, China

ARTICLE INFO

This manuscript was handled by Corrado Corradini, Editor-in-Chief, with the assistance of Patrick Lachassagne, Associate Editor

Keywords:
Runoff mechanism
Conceptual hydrological model
Subsurface runoff
Soil-epikarst systems
Karst critical zone

ABSTRACT

Southwest China receives abundant rainfall with a mean annual precipitation of 1450 mm (1960–2013) but surface runoff is small, whereas subsurface runoff is relatively large on karst hillslopes. However, not enough studies have been done to investigate the mechanisms of surface and subsurface runoff generation in subtropical karst landscapes. Here we report the dynamics of soil water content (SWC), instantaneous water levels at the soil-epikarst interface (SEI), and runoff characteristics related to the mechanisms of near-surface runoff generation at the slope scale (5 m × 20 m). Four field rainfall simulation experiments were conducted with rainfall intensities ranging from 35 to 136 mm h^{-1}. Subsurface saturation started first at the relatively flat lower slope, and then extended up slope. Subsurface runoff began after subsurface saturated areas connected to each other, representing a "fill-and-spill" mechanism. Surface runoff, which mainly developed after instantaneous water levels reached near the surface, represents an "*infiltration-excess and saturation-excess*" runoff mechanism, where two thresholds must be attained: rainfall amount and intensity. The rainfall amount threshold is dependent on soil water deficit, water capacity of the epikarst-surface depression at the SEI, and deep percolation from SEI. The rainfall intensity threshold must be larger than the steady infiltration rate of SEI, which is the prerequisite for the saturation of the epikarst-surface depression and soil layer. Steady SEI infiltration rate was estimated (40 mm h^{-1}) according to the surface runoff generation mechanism. This parameter is important as it represents the lower boundary condition in modeling hillslope hydrological processes. Rainfall-runoff thresholds for surface and subsurface runoff decrease with increasing rainfall intensity. Overall, our results show that epikarst permeability along karst hillslopes is relatively high, being the main factor controlling surface and subsurface runoff generation. Therefore, epikarst permeability significantly affects near-surface hydrological processes in karst landscapes. Our data contribute to a more comprehensive understanding of runoff generation processes and water cycle in the critical zone.

1. Introduction

Karst landscapes cover approximately 7–12% of the Earth's continental area, and about one quarter of the global population is completely or partially dependent on drinking water from karst aquifers (Hartmann et al., 2014). The karst region of southwest China is one of the world's largest areas exposed to subtropical climates with a nearly continuous karst terrain, covering a total area of 5.4×10^5 km^2 (Fu et al., 2015c). Cockpit karst is the most typical landscape style present in southwest China and is locally known as "fengcong", which is characterized by enclosed depressions of similar size surrounded by overlapping hills and ridges. The regional bedrock geology is primarily composed of dolomitic carbonatites, limestone, and intermediate types. These rocks have a dense structure, low porosity (< 3%), and low hydrochloric acid (HCl) insoluble matter (< 4%) (Yuan, 1994). Previous studies on karst slope hydrological processes were conducted in either sub-humid, semi-arid, or Mediterranean karst areas (Wilcox et al., 2008; Leh et al., 2008; Li et al., 2011). The results from these studies cannot represent humid subtropical karst near-surface hydrological regimes (Fu et al., 2015d). This region is characterized by fragile ecosystems controlled by geological (carbonate bedrock) and hydroclimatic (rainfall and temperature pattern) conditions as well as

* Corresponding authors at: 644 Yuanda 2nd Road, Changsha 410125, Hunan, China.
E-mail addresses: zyfu@isa.ac.cn (Z. Fu), hbchs@isa.ac.cn (H. Chen).

https://doi.org/10.1016/j.jhydrol.2019.124370
Received 18 July 2019; Received in revised form 14 November 2019; Accepted 15 November 2019
Available online 18 November 2019

anthropogenic activities. Thus, the region is subject to severe soil erosion and karst rocky desertification (refers to the processes and human activities that transform a karst area covered by vegetation and soil into a rocky landscape, which has had tremendous negative impacts to the environment and social and economic conditions at local and regional scales) (Jiang et al., 2014). The region is also subject to natural hazards, such as frequent floods and droughts. An analysis from Liu et al. (2014) revealed significantly enhanced precipitation extremes and flood severity across southwestern China over the past 60 years. Therefore, knowledge of the mechanisms that generate hillslope runoff in this region is fundamental to combat rocky desertification, effectively manage water resources and forecast flood disasters (Fleury et al., 2013).

Hillslopes are a fundamental landscape unit for hydrological responses and also serve as a basic building block for many watershed models (Tromp-van Meerveld and McDonnell, 2006b). Hillslope hydrology research can provide parameters for and can help to design the structure of watershed models. Integration of the hillslope structures into earth system models (ESMs) can improve ESM grid-level water, energy, and biogeochemical fluxes prediction ability (Fan et al., 2019). Moreover, despite the importance of the integrated soil-epikarst systems for karst water resources, previous research mostly focused on karst groundwater. Only a few studies that directly characterized the shallow subsurface processes of karst systems have been conducted (Berthelin and Hartmann, 2020).

In the karst region of southwest China, slopes are characterized by a thin soil layer that overlays a highly weathered bedrock surface (epikarst), which is formed by soil-filled grikes. This is similar to other landforms where irregular bedrock surface underlays a shallow soil layer (Tromp-van and McDonnell, 2006a; Graham et al., 2010). This region experiences a high mean annual precipitation (> 1450 mm) but the surface runoff (SR) coefficient on karst hillslopes consistently remains less than 5% regardless of the amount of annual rainfall (Chen et al., 2012; Peng and Wang, 2012; Qin et al., 2015). We found that deep percolation and subsurface runoff (SSR) are the dominant runoff components, accounting for 71% and 9% of the total rainfall amount, respectively (Zhu et al., 2017). In contrast, SR occupies less than 2% on karst hillslopes in southwest China in the rainy season (from July 30th to September 30th, 2015) (Zhu et al., 2017). Therefore, the area's hydrological processes mainly occur at the subsurface level. Previous studies have shown that SSR is a dominant runoff-producing mechanism in humid environments and steep terrain around the world (Weiler et al., 2005; McDonnell, 2003; Tromp-van Meerveld and McDonnell, 2006b). Although Wilcox et al. (2008) and Fu et al. (2015a,c) conducted valuable research on subsurface runoff along karst hillslopes, SR or SSR on certain karst hillslope plots have seldom been monitored through long-term natural rainfall-runoff observations (Zhu et al., 2017). Thus, the mechanisms of SR and SSR generation on karst hillslopes merit further research. This common response among various catchments may be empirically more meaningful than the particular characteristics of an experimental watershed (McDonnell, 2003).

Infiltrated water (the process by which water enters the soil pore spaces and becomes soil water) that moves laterally down a hillslope through soil layers or on the soil-bedrock interface (SBI) produces lateral subsurface runoff, which contributes to a stream (Weiler et al., 2005). Studies in the early 1990s indicated that pre-event water stored in a watershed before a rainfall event is the largest contributor (approximately 75% worldwide) to runoff in a stream. Furthermore, vertical and lateral preferential flows are common in natural soils, particularly in steep terrain (Buttle, 2005). A transient water table is rapidly generated at the SBI after the onset of a precipitation event, where this response controls the initial stage of lateral subsurface runoff due to the combined impact of three factors: (i) an increase in the hydraulic gradient, (ii) an increase in the cross-sectional flow area, and (iii) the formation of transient saturation areas across the hillslope (Weiler et al., 2005). Thus, Tromp-van Meerveld and McDonnell (2006b) proposed the "fill and spill" theory to understand the development of SSR and explain the observed threshold behavior of the Panola hillslope. Du et al. (2016) found that low angle slopes exhibit thresholds and a fill-and-spill behavior similar to steeper hillslopes. In previous studies, we discovered that SSR is an important mechanism that generates runoff through field rainfall simulation experiments in sub-tropical cockpit karst landscapes (Fu et al., 2015c,d). SSR also fluctuates considerably with the permeability and topography of the soil-epikarst interface (SEI), initial soil moisture, and rainfall intensity (Fu et al., 2015d). We also demonstrated the influence that the soil-epikarst architecture has on near-surface hydrological processes on karst hillslopes (Fu et al., 2015c). However, our previous studies were mainly focused on runoff hydrographs. In other words, our observations of SR and SSR generation mechanisms were limited due to a lack of essential monitoring equipments (Fu et al., 2015c,d), such as soil moisture or instantaneous water table monitors. In this study, we aim to determine whether our previous observations justify the fill-and-spill theory.

Fu et al. (2015d) found that SR develops only under extremely high rainfall events, and revealed that karst hillslopes produce SR from a saturation excess runoff mechanism. However, most karst slopes are characterized by a thin soil layer that overlays an epikarst surface (e.g., a soil depth of merely 10–30 cm on the hillslope) (Fu et al., 2015b). In this case, the soil layer becomes easily saturated, which should easily generate significant SR. However, in reality, the SR coefficient consistently remains below 5% during natural rainfall events (Chen et al., 2012), thus, no SR occurs during relatively small rainfall intensities, such as those in sprinkling experiments (Fu et al., 2015c,d). Therefore, the saturation excess runoff mechanism is not fully applicable to karst slope SR. Gan et al. (2016) also found that SR does not occur under a relatively small rainfall intensity on bare karst slopes. Once the rainfall intensity is large enough, however, the SR amount increases with an increase in the rainfall intensity. Therefore, numerous studies have suggested the existence of a rainfall amount threshold that, at a certain point, generates runoff (McDonnell, 2003; Tromp-van Meerveld and McDonnell, 2006b; Tromp-van and McDonnell, 2006a; Graham et al., 2010; Fu et al., 2015d). We, however, propose that there is another rainfall intensity threshold that produces SR. Moreover, Chen et al. (2012) found that the local substrate structure, rather than land use, affects SR generation (Yang et al., 2016). Several other studies have also shown that the permeability of the SBI has a significant impact on hydrological processes at the hillslope scale (Freer et al., 2002; Weiler et al., 2005; Tromp-van and McDonnell, 2006a; Graham et al., 2010; Fu et al., 2015d). Based on virtual numerical experiments, Ameli et al. (2015) suggested that the physical mechanisms associated with SSR, which derive from infiltration excess at the SBI, are similar to SR due to infiltration excess at the soil surface. Both occur on slopes characterized by a highly permeable layer with high infiltration capabilities that overlies (parallel) a low-permeability layer (e.g., bedrock). For SR, the air layer serves as the high-permeability layer and the soil layer as the low-permeable layer. Thus, the prerequisite for SSR generation is infiltration water perched at the SBI, i.e.,—the soil infiltration rate must exceed the SBI infiltration rate. Karst slope soils have a high infiltration capacity with steady infiltration rates ranging from 40 to 130 mm h^{-1} (Chen et al., 2011), allowing the infiltrated water to easily reach the SEI, which then acts as an infiltration barrier for the accumulation of water (Fu et al., 2015d). Thus, we hypothesize that the rainfall intensity threshold to yield runoff is related to the permeability of the SEI on the karst slope. Fu et al. (2015d) found that the SEI has a near-steady infiltration rate of approximately 35 mm h^{-1}. Due to the sufficiently large soil infiltration rate in karst regions, the rainfall intensity should be extremely high (larger than the SEI infiltration rate) for formation of transient saturation area, through which the subsurface saturation area can form and expand, which ultimately leads to SSR and SR. Based on these previous results, we propose a hypothesis where a rainfall intensity threshold exists, in addition to the rainfall amount threshold, to generate both SSR and SR. Moreover, the rainfall intensity threshold is

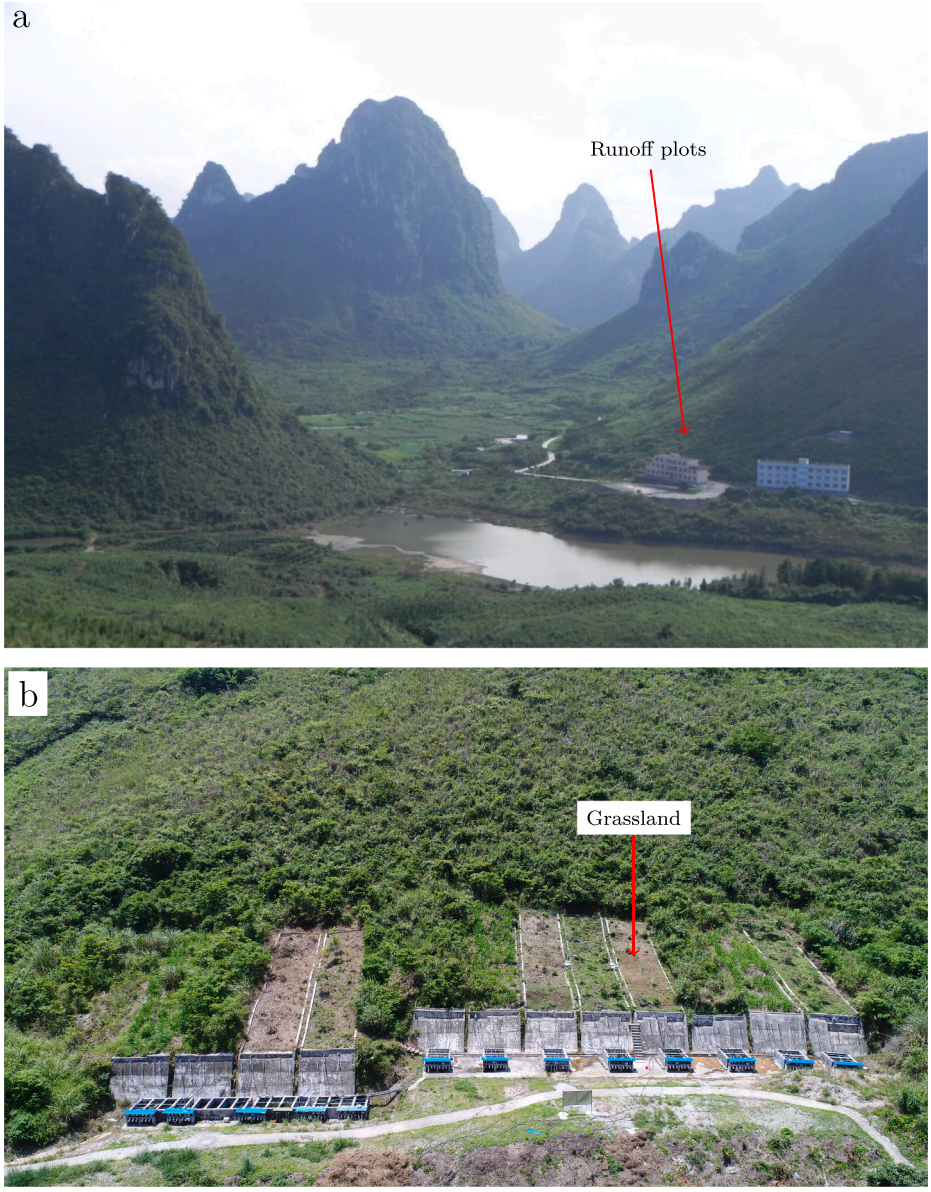

Fig. 1. The Mulian catchment (a) and runoff plots (b) in southwest China.

related to the SEI infiltration rate.

Then, the following questions guided this study:

(1) Does the fill-and-spill theory apply to the SSR generation mechanism on karst hillslopes?
(2) Does a rainfall intensity threshold exist that will generate significant SSR and SR? If so, is there a relationship between this value and the steady SEI infiltration rate?

2. Materials and methods

2.1. Experimental site description

This study was conducted in a typical karst catchment (24°43′58.9″—24°44′48.8″ N, 108°18′56.9″—108°19′58.4″ E) in Huanjiang county, which lies in northwest Guangxi (southwest China). The topographic catchment has an area of 1.46 km^2 (Fig. 1a and 2b) and andthe elevation ranges from 272 to 647 m 647 m above sea level. The watershed is representative of cockpit karst and characterized by a flat depression (30% of the watershed) surrounded by hills on three sides with an outlet in the northeast (Fig. 1a). Approximately 60% of the hillslope land has a slope greater than 25°. The near-surface karst slope soil-epikarst architecture system consists of a thin soil layer (0-50 cm) (0–50 cm) underlain by a highly irregular epikarst surface. Shallow and discontinuous soils derive from dolomite (which account for about one third in karst region of southwest China) and contain significant amounts of rock fragments. The soil type is rendzina, which has a texture between clay and clay-loam (25-50% (25–50% silt and 30-60% 30–60% clay). Soils are well-drained, gravelly, and calcareous, with stable infiltration rates ranging from 40 to 130 mm h^{-1} (Chen et al., 2012). The epikarst surface has a near-steady infiltration rate of approximately 35 mm h^{-1}, where the subsurface runoff occurs along the SEI and is dominated by preferential flow (Fu et al., 2015d). The region has a subtropical mountainous monsoon climate, with an average annual temperature and rainfall of 19.9 °C and 1,455.6 mm (1980–2013), respectively. Approximately 74% of a given year's precipitation falls during the wet season between May and September. Our previous study (Hu et al., 2015) reports more detailed information on the geohydrological conditions of this region.

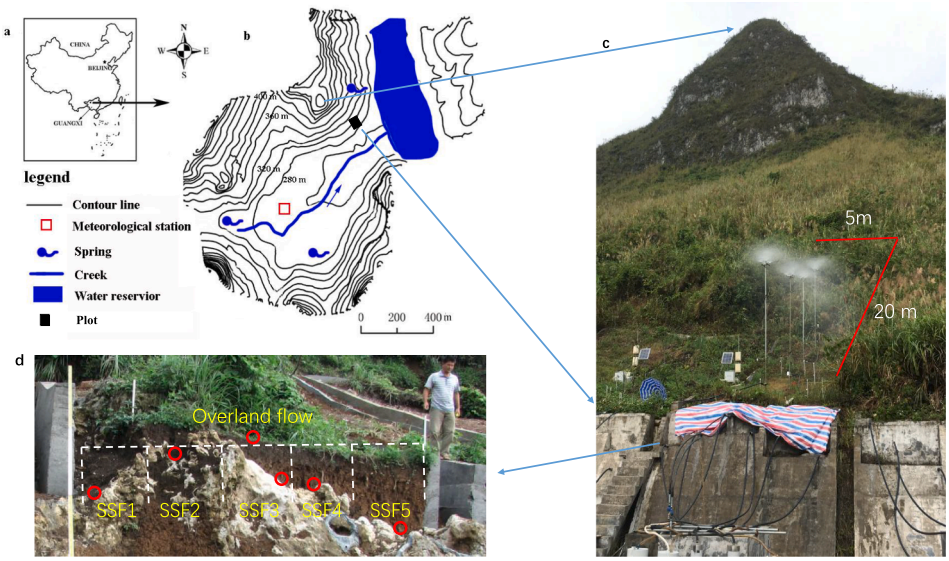

Fig. 2. (a) Location of Guangxi; (b) topographic map of Mulian catchment; (c) photograph of the slope and plot; (d) the 5-m width of the trench, which was divided into five equal sections to monitor subsurface flow.

2.2. Experimental plots

The hillslope used in this study is located on the western side of the watershed (Figs. 1 and 2). The general approach to studying subsurface runoff generation and movement in response to precipitation and snowmelt involves excavation to the SBI at the lower boundary of the experimental hillslope to expose the subsurface runoff (Tromp-van Meerveld and McDonnell, 2006b; Fu et al., 2015d). Twelve hillslope runoff plots (5 m × 20 m) were established at the lower part of the slope (Fig. 2b), each with a trench of 5 m in width (the total width of the trench was 80 m), where material was removed completely down to the unweathered bedrock (an average vertical depth of 4 m) using a backhoe. The trench site epikarst was moderately weathered with a shallow soil mantle (the mean soil thickness of the 12 plots was 50 cm based on a survey of the trenches among the 12 runoff plots). Concrete walls were installed deep into the epikarst surface on three sides of the plots (the left, right, and upper edges) to prevent SR exchange between adjacent plots.

The 12 plots were divided into four groups (corn, forage, walnut, and natural grassland) with three replicates to quantify the effects that vegetation types on water, sediments, and nutrient loss. A grassland plot (Figs. 1b and 2), which experienced very little SR and SSR, was selected for rainfall simulation experiments in this study to discern water pathway characteristics. The grassland plot soil depth was surveyed on a 1-m grid using a 10.0 mm hand auger that was vertically forced through the soil profile to the epikarst. The soil depths of the study plot range from 0 to 1.18 m with a mean value of 0.66 m and coefficient of variation of 0.60. The surface topography is planar apart from a bedrock outcrop at the lower-left corner of the plot (Fig. 2), whereas the bedrock topography is highly irregular. There are some areas of deep soils of the plot between 4–14 m upslope from the trench (Fig. 3), which are caused by large depression in the epikarst. These areas of deep soils are defined as epikarst-surface depression. Our previous study (Fu et al., 2015d) provide detailed descriptions of the trench characteristics.

Nine soil samples were collected from up, middle, and down slope positions in replicates of three to measure the soil properties. Soil particle size distributions were measured using a Mastersizer 2000 (Malvern Instruments, Malvern, England). The soil bulk density of undisturbed soil samples (BD, g cm^{-3}) was measured using steel columns (5 cm diameter, 100 cm^3 volume) via the excavation method. The rock fragment content (RFC, %) was determined as the ratio between the rock weight and dry soil weight. Soil saturated hydraulic conductivity (mm h^{-1}) was measured using the constant-head method while soil organic carbon (SOC, g kg^{-1}) was determined using the dichromate oxidation method (Fu et al., 2015d). Table 1 lists the soil and epikarst characteristics.

2.3. Rainfall simulations and data collection

Four portable rainfall simulators were used to simulate rainfall with approximately 80% uniformity. The structure of the portable rainfall simulators is described in detail by Fu et al. (2015d). Four rainfall simulation experiments were conducted between October 28 and November 4, 2016, to understand rainfall-infiltration-runoff processes. Rainfall intensity (R_i) was set to 35, 73, 100, and 136 mm h^{-1} to simulate medium to high intensity rainstorms in the region (Fu et al., 2015d). To conduct the experiments under uniform initial soil water conditions, the plot was sprinkled with 200 mm of water once daily prior to each experiment. All four rainfall simulation experiments consumed 200 mm of water and near steady runoff rates were reached at the end of the experiments. Table 2 lists the rainfall and runoff characteristics.

Eight observation points were selected to monitor the soil water content (SWC) at 10 cm, 30 cm, and the SEI based on the soil depth distribution. Six of the eight locations were monitored for the instantaneous water table at the SEI. Fig. 3 shows the locations for SWC and water level monitoring. The SWC was measured every 5 min using frequency domain decomposition (Stevens Hydra Probe Soil Sensor, Stevens, USA). Water tables at the SEI were monitored every 5 min using the water level logger (U20-001-04, ONSET, America).

The 5-m trench was divided into five equal sections and the SSR from each section was measured and recorded as subsurface runoff 1 (SSF1)-5 (SSF5) from left to right. A water pipe was fixed at the middle of the trench to collect SR. Another pipe was installed at the bottom of the trench face to measure epikarst seepage runoff (ESR), which occurred at the epikarst-bedrock interface (EBI). SR, SSR, and ESR were measured by routing the runoff through a tipping bucket flow gauge with a resolution of 100 mL (SSR) and 1 L (SR and ESR) (TB1L, Hydrological Services, USA). The lower edges of the experiment plot were covered in plastic film to prevent rainfall from dripping directly into the SR gutter (Fig. 2c).

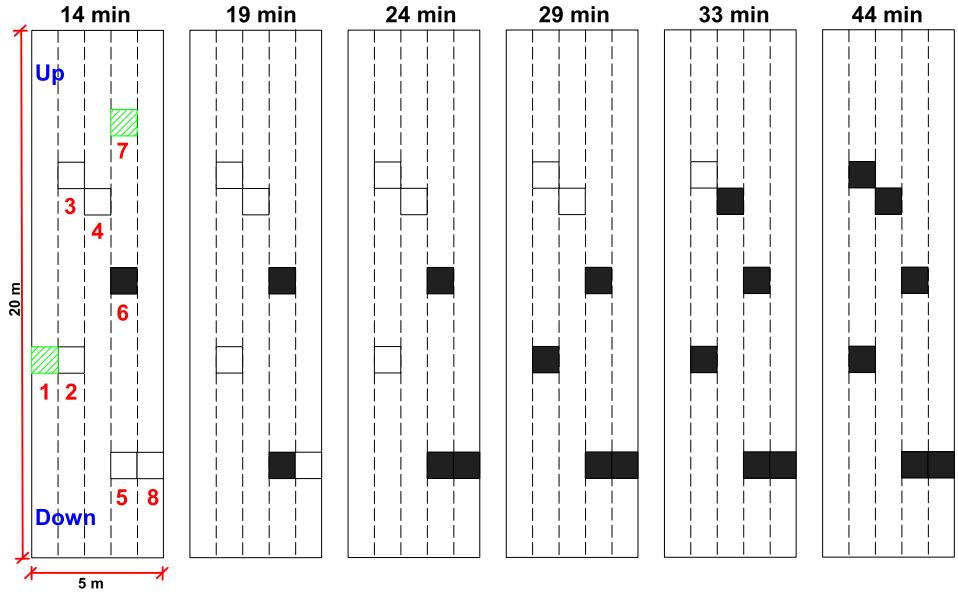

Fig. 3. The expanded saturation area at the soil-epikarst interface with rainfall intensity at 100 mm h^{-1}. (The black squares represent the locations that produced the transient subsurface saturation. 1–8 represents the equipment locations for monitoring soil water content. Locations 3, 4, and 7 are regarded as up slope, locations 1, 2, and 6 are regarded as middle slope, and locations 5 and 8 are regarded as down slope. Water levels were observed at all locations except at locations 1 and 7.).

Table 1
Soil and epikarst properties of the experimental plot.

Variables	Depth (cm)			
	0–10	10–20	20–30	30–50
Soil properties				
Rock fragment content (%)	7.4	12.8	4.1	2.3
Sand (%)	28.1	27.2	28.1	29.2
Silt (%)	43.7	39.3	35.8	36.6
Clay (%)	28.3	33.5	36.2	34.3
Bulk density (g cm^{-3})	1.0	1.1	1.1	1.0
Total porosity (%)	62.3	58.1	59.6	61.1
Capillary porosity (%)	48.4	41.5	41.7	41.9
Non-capillary porosity (%)	9.5	8.1	9.6	8.1
Saturated hydraulic conductivity (mm h^{-1})	174.2	60.4	42.0	51.2
pH	7.7	7.8	8.0	8.5
Soil organic matter content (%)	5.2	3.5	3.4	3.8
Epikarst rock properties				
Bulk density (g cm^{-3})	2.5	—	—	—
Total porosity (%)	7	8	4	3
Saturated hydraulic conductivity (mm h^{-1})	16	—	—	—

Table 2
Rainfall, subsurface runoff, surface runoff, and epikarst seepage runoff characteristics for each experimental treatment.

Variable	Rain-1	Rain-2	Rain-3	Rain-4
Date	Nov. 3	Oct. 30	Nov. 4	Oct. 28
Rainfall characteristics				
Total rainfall (mm)	200	200	200	200
Rainfall intensity (mm h^{-1})	35	73	100	136
Rainfall duration (min)	345	164	120	88
Subsurface runoff characteristics				
Threshold rainfall (mm)	41.2	51.2	48.3	34.1
Time to outlet (min)	71	42	29	15
Time to peak (min)	342	152	69	44
Rate of peak flow (mm h^{-1})	2.2	6.8	6.1	14.5
Runoff coefficients (%)	3.5	6.1	4.7	6.3
Surface runoff characteristics				
Threshold rainfall (mm)	—	72.0	51.7	40.9
Time to outlet (min)	—	57	31	18
Time to peak (min)	—	117	114	84
Rate of peak flow (mm h^{-1})	—	10.6	26.9	43.7
Runoff coefficients (%)	—	6.3	12.3	19.2
Epikarst seepage runoff characteristics				
Time to outlet (min)	117	67	49	34
Time to peak (min)	332	162	104	54
Rate of peak flow (mm h^{-1})	1.9	3.6	3.5	5.0
Runoff coefficients (%)	4.4	5.2	4.6	5.6
Total runoff coefficients (%)	7.9	17.6	21.6	31.1

3. Results

3.1. Temporal and spatial variations in SWC patterns

Table 3 lists the initial SWC at different positions and depths in the four experiments. All SWCs increased with soil depth among the three slope positions. The initial SWCs among the four experiments were compared and analyzed with a one-way analysis of variance (One-way ANOVA), which indicated that there were no statistical differences among the four experiments ($P < 0.01$). Thus, the differences in hydrological processes among the four rainfall simulation experiments are attributable to different rainfall intensities.

Rainfall intensity significantly affected variations in the SWC. Table 4 lists the SWC response times, showing that it decreased with rainfall intensity at three depths and different locations, with significant differences at certain locations. The slope position influenced the SWC response times at the SEI (Table 5) from the down slope to middle slope, and, finally, to the upper slope. These differences were not significant at the highest rainfall intensity (136 mm h^{-1}).

Figs. 4a–c and 5a–c, respectively, show the SWC characteristics for rainfall intensity at 35 and 100 mm h^{-1}. At different depths and slope positions, the SWC changed rapidly, i.e., rapid increase during the onset of precipitation and rapid decline quickly after the rain had stopped, at which point they returned to the original levels prior to precipitation within 24 h. These observations indicate a low soil water storage capacity and rapid hydrological processes on karst hillslopes. In the SEI, the SWC was sustained longer than at the top soil layers and significantly longer at middle and down slope areas compared with the up slope area. This may be attributed to the lateral movement of infiltrated water and finer soil textures at deeper soil layers, which are characterized by higher water holding capacities at greater depths below

Table 3
Initial soil water content of the four rainfall simulation experiments.

	Rainfall-1			Rainfall-2			Rainfall-3			Rainfall-4		
	10 cm	30 cm	Int	10 cm	30 cm	Int	10 cm	30 cm	Int	10 cm	30 cm	Int
Up-3	0.223	0.355	0.328	0.223	0.362	0.343	0.226	0.361	0.340	0.222	0.362	0.343
Up-4	0.336	0.360	0.342	0.341	0.367	0.359	0.347	0.364	0.357	0.349	0.371	0.359
Up-7	0.312	0.390	0.268	0.318	0.398	0.279	0.318	0.397	0.278	0.325	0.404	0.282
Mid-1	0.333	0.404	0.452	0.342	0.413	0.466	0.341	0.410	0.468	0.338	0.412	0.464
Mid-2	0.271	0.348	0.513	0.277	0.355	0.529	0.276	0.353	0.530	0.272	0.356	0.535
Mid-6	0.293	0.432	0.446	0.300	0.444	0.474	0.305	0.440	0.468	0.296	0.441	0.475
Down-5	0.348	0.443	0.535	0.354	0.448	0.542	0.356	0.448	0.544	0.352	0.447	0.539
Down-8	0.294	0.481	0.554	0.300	0.486	0.563	0.300	0.485	0.564	0.293	0.490	0.564

Int: the soil-epikarst interface; Up-3, Up-4, and Up-7 represent the soil water contents monitored at three up slope positions; Mid-1, Mid-2, and Mid-6 represent the soil water contents monitored at three middle slope positions; Down-5 and Down-8 represent the soil water contents monitored at two down slope positions, which are presented in Fig. 2.

Table 4
The effects of rainfall intensity on the response time of the soil water content (min).

Position	35 mm h^{-1}	73 mm h^{-1}	100 mm h^{-1}	136 mm h^{-1}
Upper slope				
10 cm	20.3 a	17.0 a	14.0 a	9.0 a
30 cm	28.7 a	23.7 ab	19.0 ab	12.3 b
SEI	79.5 a	52.0 b	42.3 b	24.0 c
Middle slope				
10 cm	22.0 a	15.3 ab	17.3 ab	10.7 b
30 cm	40.3 a	25.3 b	20.7 bc	15.7 c
SEI	70.3 a	35.3 b	29.0 bc	22.3 c
Down slope				
10 cm	22.0 a	14.5 b	14.0 b	9.0 c
30 cm	44.5 a	24.5 b	16.5 b	16.5 b
SEI	49.5 a	27.0 b	21.5 bc	19.0 c

Different letters denote the significant difference at $P < 0.05$ (LSD test).

Table 5
Response times of the soil water content at the soil-epikarst interface at different slope positions (min).

Position	Upper slope	Middle slope	Down slope
35 mm h^{-1}	79.5 a	70.3 a	49.5 b
73 mm h^{-1}	52.0 a	35.3 b	27.0 c
100 mm h^{-1}	42.3 a	29.0 b	21.5 c
136 mm h^{-1}	24 a	22.3 a	19.0 a

Different letters denote significant difference at $P < 0.05$ (LSD test).

the surface.

3.2. Water levels at the soil-epikarst interface

The transient water levels at the SEI represented the temporal and spatial patterns of transient saturation at the SEI while the Water levels (WLs) at the SEI relate to SSR initiation and generation at the trench face (Tromp-van Meerveld and McDonnell, 2006b) (Fig. 3). Similar to the SWC, the WL response times decreased with rainfall intensity (Table 6), indicating that the subsurface saturation areas formed rapidly under high rainfall intensity. The WL response times had the following orders: w6 (88 cm), w5 (120 cm), w8 (141 cm), w2 (138 cm), w4 (145 cm), and w3 (139 cm) (Fig. 3). Subsurface saturation areas were generated from the down slope to upper slope. Response time w6 responded first because it had the shallowest depth (88 cm).

The WLs began to decline after rainfall had stopped and disappeared within 18 h (Fig. 5d). The disappearing times had the following order: w3, w4, w6, w5, w8, and w2. The subsurface saturation areas vanished from the upper slope to down slope.

3.3. Surface and subsurface runoff hydrographs

Fig. 6a shows the time for runoff to occur (SR, SSR and ESR plotted against the rainfall intensity for different treatments. A negative exponential function was used to fit the curves (Zhao et al., 2014). Both regression equations passed the test of significance ($p < 0.05$), indicating that they precisely capture the negative relationship between these two parameters. In other words, the time to runoff decreases with rainfall intensity. The relationship between the time to peak discharge (SSR, SR, and ESR) and rainfall intensity is similar to the relationship between time to runoff and rainfall intensity, which can also be described using the negative exponential function (Fig. 6b). Runoff coefficients (R_c) of SR increased with rainfall intensity (R_i) ($R_c = 0.203 \times R_i - 8.377$, $R^2 = 0.998$, $P < 0.05$, $F = 447.9$). These observations suggest that more rainfall was converted to SR under high rainfall intensity. The increase in SR with increasing rainfall intensity was concordant with previous observations (Chaplot and Bissonnais, 2003; Zhao et al., 2014).

Figs. 4e, f and 5e, f show runoff hydrographs for relatively low (35 mm h^{-1}) and high (100 mm h^{-1}) levels of rainfall intensity, respectively, consisting of SR, SSR, and ESR. SSR and ESR dominated runoff processes under low rainfall intensity. SR was not observed in the lowest rainfall intensity event (35 mm h^{-1}) but did occur with increasing amounts as rainfall intensity increased (Table 2, Figs. 4 and 5). SR occurred later than SSR in all rainfall events (Table 2).

Rainfall intensity exerted a significant effect on the hydrograph shapes of SR, SSR, and ESR (Figs. 4f and 5f). The hydrograph was flat for lower rainfall intensity but fairly steep for high rainfall intensity. The peak SSR rates were 2.2, 6.8, 6.1, and 14.5 mm h^{-1} while the ESR rates were 1.9, 3.6, 3.5, and 5.0 mm h^{-1} with rainfall intensities of 35, 73, 100, and 136 mm h^{-1}, respectively. The individual SSR characteristics were similar to those of the total SSR as discussed above.

Table 7 summarizes the negative relationship between time to runoff and time to peak runoff for each individual SSR and rainfall intensity, which can also be described using a negative exponential function. Both time to runoff and time to peak runoff followed a similar order regardless of rainfall intensity, i.e., SSF5, SSF4, SSF3, and SSF1.

4. Discussion

4.1. Variations in the SWC and water table at the SEI

The soil water content at a depth of 10 cm was less than that at 30 cm and the SEI, which can be attributed to differences in the soil texture and saturated hydraulic conductivity between the soil at 10 cm and that at 30 cm and the SEI. As summarized in Table 1, the soil sand contents were identical at 10 (28.1%) and 30 cm (28.1%) but the soils at 30 cm had increased clay contents, with an average of 36.2% compared with the clay content at 10 cm that had an average of 28.3%.

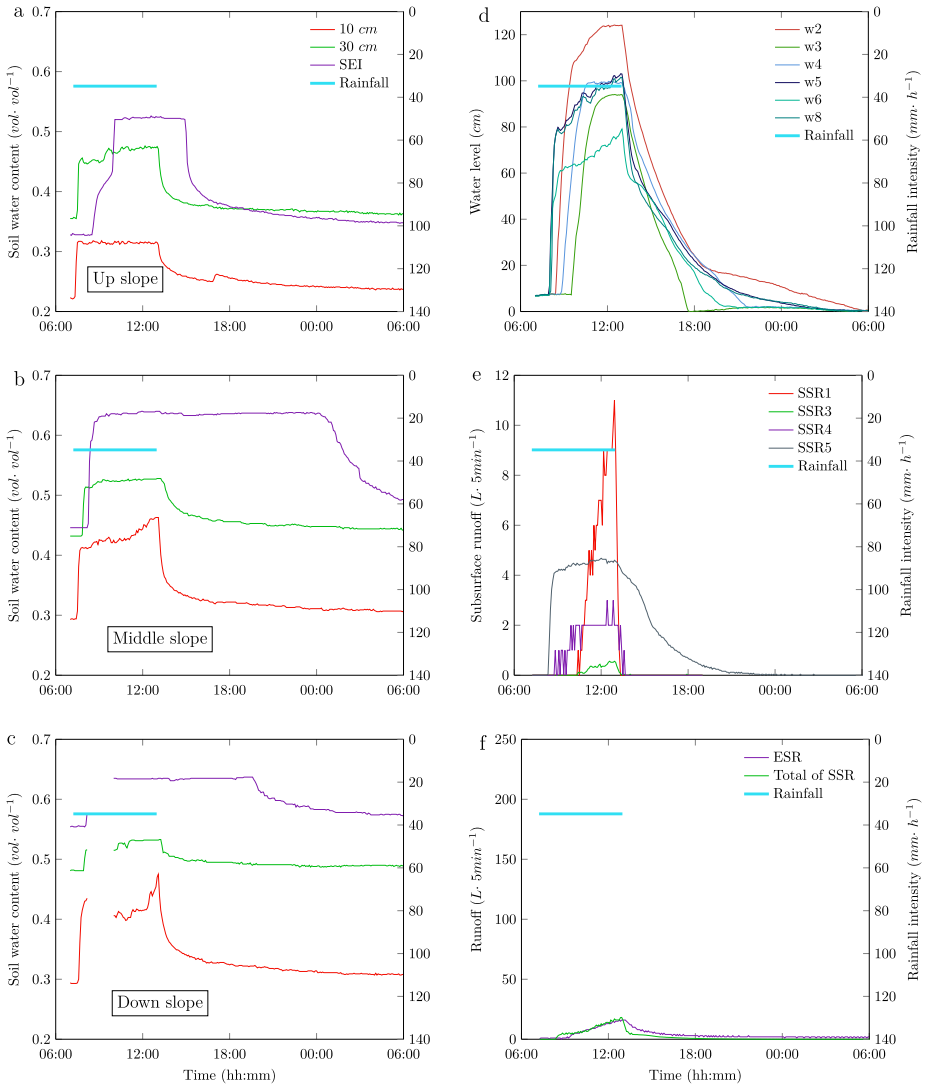

Fig. 4. Rainfall intensity of 35 mm h^{-1}. Soil water contents at different slope positions (a–c), water levels at the soil-epikarst interface (d), subsurface runoff (e), and epikarst seepage runoff (f).

Moreover, the soils at 10 cm had a greater saturated hydraulic conductivity, with an average of 174.2 mm h^{-1}, compared with that at 30 cm, with an average of 42.0 mm h^{-1}. Finally, the saturated hydraulic conductivity of the SEI was the lowest (16.0 mm h^{-1}) compared with the soils at 10 and 30 cm. Therefore, the infiltration water perched at the SEI while lateral subsurface runoff contributed to the delay in soil water depletion at the SEI. All of these reasons caused the soil water content at 10 cm to be less than that at 30 cm and the SEI.

SWC response times showed a positive correlation with rainfall intensity, indicating that the infiltration rate increased with rainfall intensity in our experiments. However, the effect that rainfall intensity had on the infiltration rate was inconsistent. On certain soils, surface seals decreased the infiltration rates with increases in the rainfall intensity (Dunne et al., 1991). Nevertheless, a larger soil infiltration capacity than the rainfall intensity was maintained during most rainfall events due to the higher mean soil saturated hydraulic conductivity (54.9 cm h^{-1}) in the karst area of our experiment site compared with non-karst areas (2.55 cm h^{-1} for loess soil and 0.03 cm h^{-1} for glacial till soil) (Wang et al., 2016). Thus, the SWC response times decreased with rainfall intensity. The upslope region in the study area is steeper than the down slope region. Therefore, infiltration water moved laterally from the up slope to the down slope, where the SWC at the SEI first changed at the down slope and, subsequently, at the up slope.

The SWC and transient water level at the SEI rapidly changed throughout our experiments (Figs. 4a–c and 5). The thin soil layer, relatively high hydraulic conductivity, and presence of several fissures, gaps, channels, and sinkholes lead to a poor water holding capacity and rapid hydrological processes in the karst area. Although the region has a subtropical mountainous monsoon climate with a large amount of annual precipitation (more than 1,200 mm), the karst terrain lacks sufficient soil water for vegetation growth (Fu et al., 2015; Wang et al., 2016, 2017). This unique drought phenomenon, which is not induced by climatic, but rather, geological conditions, is defined as “karst drought” (Chen and Wang, 2004). We note that all experiments were conducted in November 2016, during which rapid hydrological processes resulted in fairly similar initial SWCs at different layers and slope positions (Table 3), providing further evidence that the soil has a low water retention capacity.

4.2. Subsurface runoff generation mechanism

SSR is the primary runoff components in humid environments with steep terrain (Weiler et al., 2005; Fu et al., 2015c,d). Tables 5 and 6 list the response time of the SWC and water tables, respectively, at the SEI. Previous studies have shown that the development of the lateral transient water level at the SEI controls the onset of lateral SSR due to the

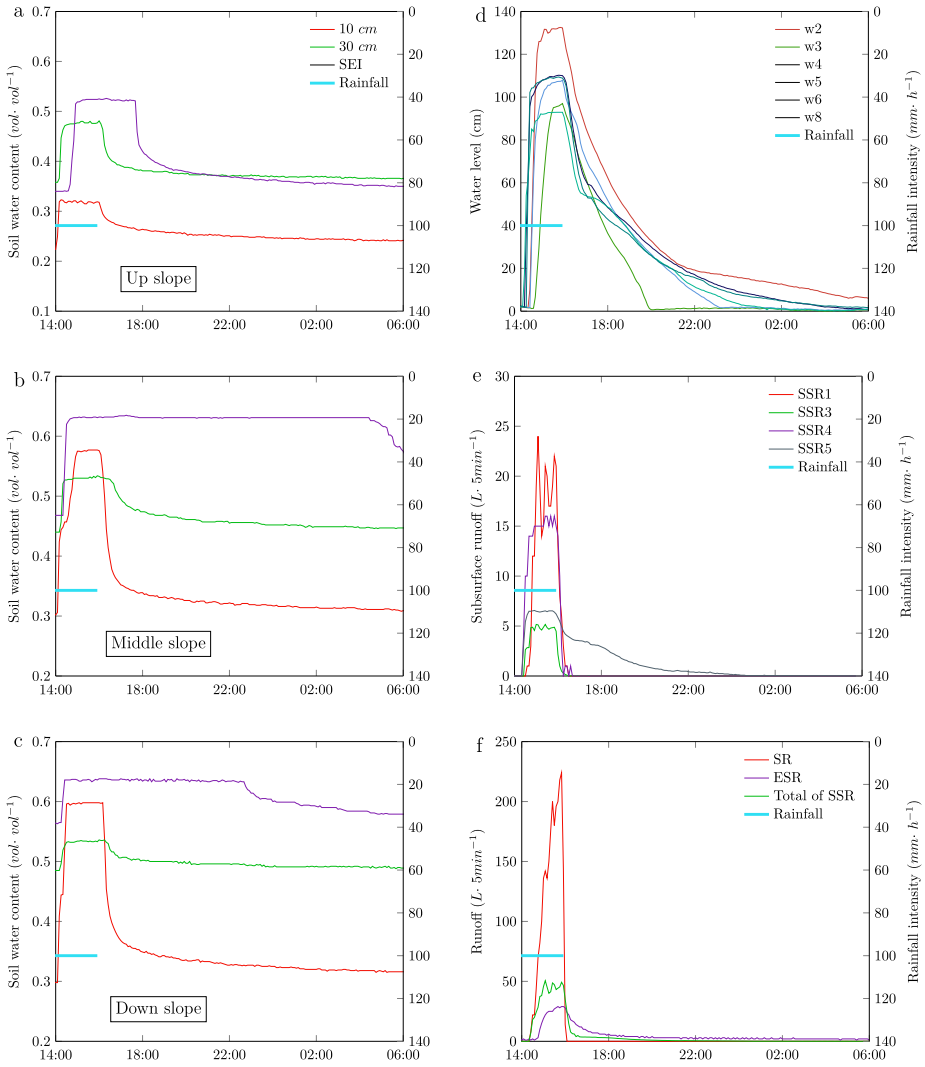

Fig. 5. Rainfall intensity of 100 mm h^{-1}. Soil water contents at different slope positions (a–c), water levels at the soil-epikarst interface (d), subsurface runoff (e), and epikarst seepage runoff and surface runoff (f).

Table 6
The response times of the water level at the soil-epikarst interface at different rainfall intensities (min).

Water levels	w2	w3	w4	w5	w6	w8
35 mm h^{-1}	77	142	97	47	47	47
73 mm h^{-1}	37	62	42	22	22	22
100 mm h^{-1}	29	44	33	19	14	24
136 mm h^{-1}	24	24	14	14	14	14

The water level monitoring locations are listed in Fig. 3.

combined effect of several factors: an increase in hydraulic gradient, increase in the cross-sectional flow area, and the accumulation of subsurface saturation areas across the SEI (Weiler et al., 2005; Tromp-van Meerveld and McDonnell, 2006b). Based on our observations of the transient subsurface water tables when exposed to rainfall intensities of 100 mm h^{-1} (Fig. 3 and Table 6), we found that the subsurface saturation area first formed at the down slope and then expanded upward. When the subsurface saturation area at the middle and down slopes connected with each other 29 min after the onset of rainfall, this instantaneously generated an individual SSR (SSF4 and SSF5). All observed individual SSR began 39 min after the subsurface saturation area expanded to the up slope. The time to peak SSR occurred 69 min after the onset of rainfall, suggesting that all subsurface saturation areas were connected across the entire slope at that time. The expansion of the subsurface saturation area from the down slope to the up slope is inconsistent with the conclusion of Tromp-van Meerveld and McDonnell (2006b), who observed the opposite. This can be explained where the down slope is gentler than the up slope in our study area, which allowed infiltrated water at the down slope to perch at the SEI, expanding the saturation area up slope. Tromp-van Meerveld and McDonnell (2006b), obtained a contrary result because the up slope was gentler than the down slope. The relative gradient position of the slope controls the direction in which the saturation area expands. The observed development of SSR agrees with the "fill and spill" theory proposed by Tromp-van Meerveld and McDonnell (2006b): infiltration water perches at the depression area of SEI, after which water tables reach the edge of the depression (filling process) and spill downslope over the epikarst surface towards the trench face (spilling process) as SSR continues until the disparate subsurface saturation areas accumulate into one area. The rapid increase in the runoff rate (Figs. 4d and 5d) indicates that spilling processes were triggered immediately after most epikarst-surface depressions filled. The sharp decrease in the flow rate suggests that spilling processes ceased when rainfall ceased (Figs. 4d and 5d). Thus, the fill and spill theory reflects the mechanism that generates SSR and corresponding threshold phenomenon on karst hillslopes in this area.

Our calculated SSR coefficients were quite small even when rainfall

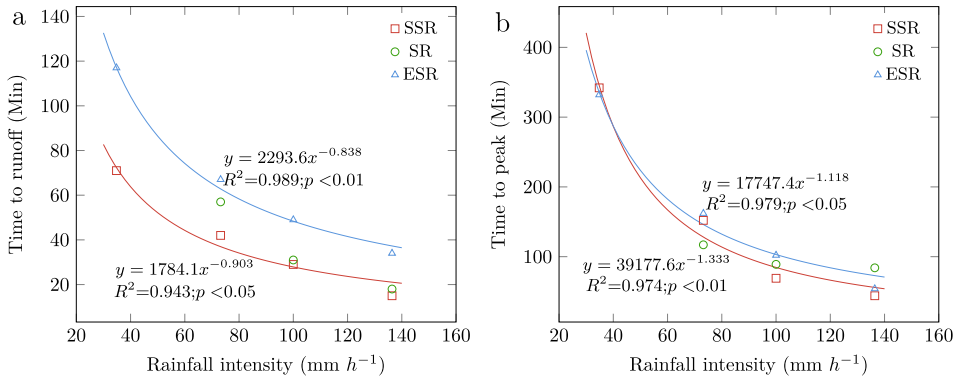

Fig. 6. Effects of the rainfall intensity on the time to runoff (min) (a); and time to peak (min) (b).

Table 7
The time to runoff and time to peak of each individual subsurface runoff at different rainfall intensities (min).

Rainfall	35 mm h^{-1}	73 mm h^{-1}	100 mm h^{-1}	136 mm h^{-1}
SSF1	192 (342)	57 (157)	39 (69)	24 (44)
SSF2	—	—	—	—
SSF3	192 (322)	47 (157)	34 (64)	14 (44)
SSF4	97 (312)	47 (122)	29 (89)	19 (44)
SSF5	67 (300)	42 (117)	29 (59)	14 (44)

The values within parentheses are the times to the peak of each individual subsurface runoff.

intensity was high (Table 2), particularly in comparison with the results of Fu et al. (2015d). This is due to the fact that we observed significant SSR discharge from the adjoining runoff plots during the experiments, which had not been counted, inducing the low total runoff coefficients. Accordingly, the concrete walls did not affect the downslope movement of SSR, proving that the underground hydrological connectivity of the plots was not affected by the facility. This can be attributed to an inherent characteristic of karst slopes, i.e.,—the abundance of fissures, conduits, caves, and sinkholes (Qin et al., 2015), suggesting that the concrete walls were unable to restrict SSR. However, no concrete walls were installed in the study plot analyzed in Fu et al. (2015d). Furthermore, Fu et al. (2015d) monitored SSR at a trench face with a width greater than 7 m, which encompassed the entire SSR.

Direct observation of subsurface saturation area expansion is difficult. Therefore, a secondary technique is required to validate the fill and spill behavior in our study area. A potential method is the use of ground penetrating radar (GPR), which is a fast, nondestructive, and efficient geophysical measurement technique. GPR has been widely used to map subsurface features. For example, Guo et al. (2014) revealed a subsurface lateral preferential flow network via GPR in a hillslope fairly similar to our study area. We hope to verify the fill-and-spill hypothesis using GPR in the future.

4.3. Surface runoff characteristics on karst hillslopes and implications

Several studies have shown that the SR coefficient increases with rainfall intensity, such that a linear relationship exists between them (Zhao et al., 2014, 2015). According to our regression analysis of the SR coefficients (R_c) and rainfall intensity (R_i) ($R_c = 0.203 \times R_i - 8.377$, $R^2 = 0.998$, $P < 0.05$, $F = 447.9$), the intercept of the trend curve at the horizontal coordinate is 41.3 mm h^{-1}, which represents the rainfall intensity threshold that generates SR at the experiment plot. This value is consistent with the previous results (Fu et al., 2015c,d; Peng et al., 2019). We infer that this value tends to exceed the rainfall intensity of most precipitation events in this region. Therefore, most studies in this region (Chen et al., 2012; Peng and Wang, 2012; Qin et al., 2015) have reported SR coefficients of less than 5% at hillslope scale regardless of annual precipitation, which is much lower than that in non-karst areas. Peng et al. (2019) found that SR requires rainfall intensities between 30 mm h^{-1} and 50 mm h^{-1}. Our previous study (Fu et al., 2015d) investigated the same site as this study found no observable SR with a rainfall intensity of 46 mm h^{-1}. We also found that the epikarst surface has a near-steady infiltration rates of approximately 35 mm h^{-1}. The relatively high hydraulic conductivity of the overlying soil (stable infiltration rate varying from 42 to 126 mm h^{-1} and mean surface soil saturated hydraulic conductivity of 552 mm h^{-1}), the existence of karst fissures and bedrock outcrops, and the thin soil layer (Wang et al., 2016) all enabled rainfall percolated into the underlying bedrock when the rainfall intensity was lower than the SEI infiltration rate. As rainfall intensity increased and ultimately exceeded the SEI infiltration rate, infiltrated water accumulated at the SEI, which led to the formation of the subsurface saturation area and generation of SR after soil layer saturation. Thus, three distinct requirements should be fulfilled for the development of SR on karst hillslopes: rainfall intensity larger than the infiltration rate of the epikarst surface, rainfall amounts exceeding the threshold (including the soil layer water capacity, water storage via epikarst-surface depressions, and deep percolation), and a slope that is not too steep to allow ponding of infiltrated water at the SBI to fill the soil layer. Similarly, when these conditions were not met, previous studies did not observe SR even during high rainfall intensity or laterally generated SSR (Fu et al., 2015c,d; Peng et al., 2017). The limited water storage capacity of the thin soil layer when exposed to sufficient rainfall, high rainfall intensity, and gentle terrain slopes all contributed to the generation of SR in our experiments, as well as during our previous studies Fu et al. (2015c,d). On the other hand, at the catchment scale, we conclude that less SR yield and flow concentration on karst slopes, which causes rapid water transit from the surface to aquifers, produces fast, localized vertical water movement, thereby enhancing groundwater recharge (Hartmann et al., 2017) and possibly inducing waterlogging.

4.4. Steady SEI infiltration rate

SR was generated 31 min after the subsurface saturation area expanded upslope, where the transient water tables at the middle and down slope areas were nearly consistent with the soil depth. These observations correspond to the saturation-excess mechanism of SR (Table 6, Figs. 4 and 5) Fu et al., 2015d).

A Spearman's rank correlation analysis was conducted to determine the response time patterns of the SWC, water tables at the SEI, and SSR in the four rainfall simulation experiments (Table 8), which indicated that soil water at different depths, transient water tables at the SEI, and SSR responded in an identical order, confirming that the previous analysis (such as the saturated area expanded pattern presented in Fig. 2) was universal.

We used the results discussed above to develop a method to estimate the steady SEI infiltration rate. The time frames necessary to generate

Table 8
Spearman's rank correlation between the response time of soil water content, water levels at the SEI, and subsurface runoff at different rainfall intensities.

Rainfall	35 mm h^{-1}	73 mm h^{-1}	100 mm h^{-1}	136 mm h^{-1}
10 cm	0.664*	0.684*	0.752*	0.408
30 cm	0.485	0.586*	0.537*	0.491
SEI	0.862*	0.796**	0.776*	0.609
Water-level	0.900**	0.900**	0.876**	0.735
Runoff	0.606	0.777*	0.798*	0.667*

**:$P < 0.01$, * : $P < 0.05$.

SR were 57, 31, and 18 min, while the times to generate SSR were 42, 29, and 15 min under rainfall intensities of 73, 100, and 136 mm h^{-1}, respectively. The time required to generate SR was nearly identical to that required to generate SSR (i.e., all individual trenches began to yield SSR 57 min after the onset of rainfall for a rainfall intensity of 73 mm h^{-1}). The initial SWC was the same for the four rainfall experiments (Table 3). Therefore, the soil layer required an identical level of water deficit to generate the SR. The second and third rainfall simulation experiments were used to estimate the infiltration rate while the fourth was used to validate it. The steady SEI infiltration rate can be expressed as "x" (mm h^{-1}). We derived the following expression according to the uniform water deficit:

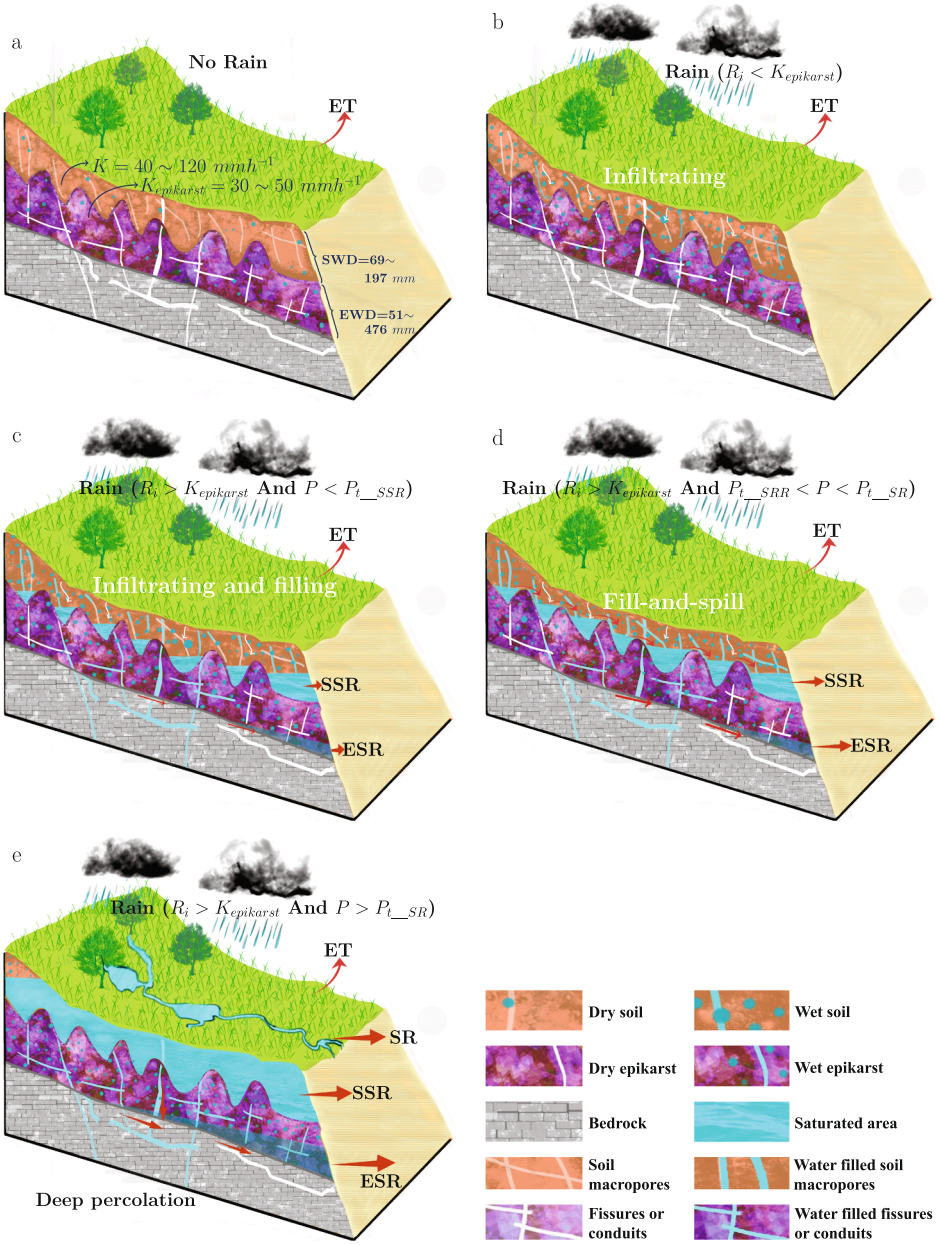

Fig. 7. Slope scale conceptual hydrological models for the integrated soil-epikarst system during no-rain periods (a) and during rainy periods, when $R_i < K_{SEI}$ (b), when $R_i > K_{SEI}$ and $P < P_{t\_SSR}$ (c), when $R_i > K_{SEI}$ and $P_{t\_SRR} < P < P_{t\_SR}$ (d), and when $R_i > K_{SEI}$ and $P > P_{t\_SR}$ (e). SWD: soil water deficit (estimated from field capacity, wilting point, and mean soil depth); EWD: epikarst water deficit (estimated from mean effective porosity of epikarst and mean epikarst depth); ET: evapotranspiration; R_i: rainfall intensity; SR: surface runoff; SSR: subsurface runoff; ESR: epikarst seepage runoff. P_{t_SRR} and P_{t_SR} are depend on initial soil-epikart system water content and R_i. Size of arrows reflects relative magnitude of fluxes.

$$\underbrace{\Big(\underbrace{73}_{\text{Rainfall intensity}} - \underbrace{x}_{\text{Infiltration rate}}\Big)\frac{mm}{h} \times \underbrace{\frac{57}{60}h}_{\text{Time to runoff}}}_{\text{Soil water storage and filling on epikarst-surface depression}} = (100-x)\frac{mm}{h} \times \frac{31}{60}h$$

$$\Downarrow$$

$$x = 41\,mm\,h^{-1}$$

We estimated the steady SEI infiltration rate to be 41 mm h^{-1} with a soil water deficit of 30.4 mm. We then used these values to estimate the time necessary to produce SR under a rainfall intensity of 136 mm h^{-1}, i.e., 19 min, which is nearly identical to the observed value (18 min). Moreover, this value was nearly equal to the rainfall intensity threshold (41.3 mm h^{-1}) required to produce SR, described in subSection 4.3. Therefore, this estimated value is reasonable. The value is slightly larger than that reported in our previous study (Fu et al., 2015c) (38 mm h^{-1}), which is likely due to the different scales used (point scale in our previous study versus a plot scale in this study). Furthermore, although the rainfall intensity in the first experiment (35 mm h^{-1}) was less than the SEI infiltration rate, the runoff coefficient of SSR was minimal but not zero (3.5%). This is because the estimated infiltration rate was the mean value of the experiment plot and depended on the weathering degree of the bedrock with a certain degree of spatial variability (Yang et al., 2016), which allowed for only a small amount of SSR. We also note that this value is useful in developing hillslope hydrological models as it represents the bottom boundary condition.

The relatively high infiltration capacity of the SEI (41 mm h^{-1}) decreases the likelihood of infiltrated water ponding at the interface to produce subsurface saturation areas. This does not readily generate SR and SSR on certain karst hillslopes (Chen et al., 2012; Fu et al., 2015d; Zhu et al., 2017). The mechanism of SR generation is an "infiltration-excess and saturation- excess" mechanism, where the "infiltration excess" reflects rainfall intensity larger than the infiltration capacity of the SEI; "saturation excess" implies that rainfall exceeds the soil water deficit, water capacity of epikarst-surface depression, and deep percolation from the interface. This mechanism corresponds to two thresholds for SR generation: rainfall amount and intensity. This could be generalized to the entire karst slopes of Southwest China, as it is consistent with the lower SR coefficients reported by many studies (Chen et al., 2012; Peng and Wang, 2012; Qin et al., 2015; Gan et al., 2016; Zhu et al., 2017).

The rainfall-runoff thresholds were 69.5, 51.7, and 40.9 mm for SR and 51.2, 48.3, and 34.1 mm for SSR at rainfall intensities of 73, 100, and 136 mm h^{-1}, respectively, showing decreases with rainfall intensity. This is because differences between rainfall intensity and the steady SEI infiltration rate (41 mm h^{-1}) increased as rainfall intensity increased. Thus, there was a decrease in the time required for the infiltrated water to fill the epikarst-surface depressions at the SEI (to produce SSR) and exceed the soil water deficit (both necessary for SR production). This reduced the amount of deep percolation, whereas water stored in the soil and epikart surface depressions remained constant.

4.5. Slope scale conceptual hydrological models for the soil-epikarst system

Finally, we propose a conceptual hydrological model to describe the particular surface-underground 'double layer' and three-dimensional hydrogeological structures and runoff components (SR, SSR, and ESR) generation mechanisms for karst hillslopes (Fig. 7). There are three layers from top to bottom: the uppermost horizon b is usually the thin soil layer (that sometimes contains rock outcrops). It is discontinuous and has a high hydraulic conductivity (26–255 mm h^{-1}). The middle horizon is the epikarst layer, having a highly irregular surface topography. Its depression area has water holding capacity, and the layer contains various water leakage structures (e.g., fissures, conduits, and sinkholes). The bottom layer is the bedrock layer and is unweathered. SR occurs at the soil surface (Fig. 7: SR), SSR occurs at the SEI (Fig. 7: SSR), and ESR occurs at the EBI (Fig. 7: ESR). Because the hydraulic conductivity of soil (26–255 mm h^{-1}) is higher than that of the epikarst ($K_{epikarst}$, 30–50 mm h^{-1}), rainfall rapidly infiltrates and reaches the SEI, accumulates in the depression area of the SEI, until instantaneous water tables at the depression area reach the edge of the depression (filling process) (Fig. 7c: Infiltrating and filling). It spills downslope over the epikarst surface towards the trench face (spilling process) (Fig. 7d: Fill-and-spill), and SSR at the SEI continues until the isolated subsurface saturation areas coalesce into one and reach the SSR rainfall amount threshold, P_{t_SSR}. When the instantaneous water tables reach the soil surface (indicating soil layer saturation, reaching the SR rainfall amount threshold, P_{t_SR}), SR occurs. When the rainfall is large enough (no matter the R_i), and percolates into epikarst fissures or conduits, ESR may occur (at EBI), as we observed that ESR occurs earlier than SSR (Fig. 4f and 5f). Soil water deficit (estimated from field capacity, wilting point, and mean soil depth) and epikarst water deficit (estimated from mean effective porosity of epikarst and mean epikarst depth) are also provided in Fig. 7a.

The conceptual hydrological model is divided into no-rain (Fig. 7a) and rainy day (Fig. 7b–e), and the rain events are characterized by their intensities (R_i) and amounts:

No-rain periods:soil-epikarst-system water storage decreases due to evapotranspiration (Fig. 7a);
Rain periods:
$R_i < K_{epikarst}$: when the R_i is smaller than the SEI infiltration rate—regardless of the rainfall amount—no subsurface saturation areas can be generated in this case (ESR may be generated if the rainfall amount is large enough and percolates into epikarst fissures and conduits, Fig. 7b);
$R_i > K_{epikarst}$ and $P < P_{t\_SSR}$: when the R_i is larger than the SEI infiltration rate, and the rainfall amount is smaller than the SSR rainfall threshold, subsurface saturated areas will occur but cannot connect with each other, thus no SSR is generated (Fig. 7c);
$R_i > K_{epikarst}$ and $P_{t\_SRR} < P < P_{t\_SR}$: when the R_i is larger than the SEI infiltration rate, and the rainfall amount is larger than the SSR rainfall threshold and smaller than the SR rainfall threshold, the subsurface saturated areas will occur and connect with each other, generating significant SSR, which agrees with the fill-and-spill theory (Fig. 7d);
$R_i > K_{epikarst}$ and $P > P_{t\_SR}$: when the R_i is larger than the SEI infiltration rate, and the rainfall amount is larger than the SR rainfall threshold, then SSR and SR will occur (Fig. 7e).

5. Conclusions

The SR coefficient consistently remains less than 5% on karst hillslopes in southwest China, regardless of the amount of annual rainfall

and vegetation types. From the hillslope hydrology perspective however, steep and thin soil mantled karst hillslopes are typically readily saturated and generate surface runoff consisting of saturated overland flow. This produces a logical paradox with the objective reality. Therefore, in order to solve this paradox, plot-scale field rainfall simulation experiments were conducted on a karst hillslope in a humid, sub-tropical, cockpit karst region of southwest China. The results indicated that SSR was generated after subsurface saturation areas (at the SEI) connected with each other. Then the "fill and spill" theory explains this process reasonably well. SR mainly developed after instantaneous water levels reached near the surface, representing an "infiltration-excess and saturation-excess" runoff mechanism. This verified our hypothesis that a R_i threshold exists, in addition to the rainfall amount threshold, which generate SR. The rainfall amount threshold consists of three components: filling of the epikarst-surface depressions at the SEI, eliminating the soil water deficit, and the amount of deep percolated water during the process. The R_i threshold must exceed the steady SEI infiltration rate, which is the prerequisite for the saturation of epikarst-surface depression and soil layers. The steady SEI infiltration rate in this study was 41 mm h^{-1}, which mostly exceeded the natural R_i in this region. It is the main factor responsible for the lower SR and SSR coefficients. The steady SEI infiltration rate may vary with hillslopes because of the high spatial variability; however, we believe that the value is large enough among karst regions, because the low SR coefficient has been observed at different slopes in karst region of southwest China.

Furthermore, a conceptual hydrological model was presented to describe the generation mechanisms of runoff components (SR, SSR, and ESR) for this complex and integrated soil-epikarst system.

These findings are based only on four rainfall simulation experiments on the foot slope of a dolomite karst hillslope. Therefore, a strict generalization, that runoff characterizes all different karst hillslopes or different hillslope positions, cannot be made. Further research should focus on the quantification of soil-epikarst architectures and associated hydrological functions along this cockpit karst hillslope. We believe that these results contribute to a more comprehensive understanding of runoff generation characteristics for karst hillslopes, and will be useful in improving the prediction ability of the earth system models.

CRediT authorship contribution statement

Sheng Wang: Conceptualization, Methodology, Investigation, Writing - original draft. **Zhiyong Fu:** Data curation, Writing - review & editing. **Hongsong Chen:** Supervision, Funding acquisition. **Yunpeng Nie:** Writing - review & editing. **Qinxue Xu:** Investigation.

Declaration of Competing Interest

The authors declare that they have no known competing financial interests or personal relationships that could have appeared to influence the work reported in this paper.

Acknowledgments

This study was financially supported by the National Natural Science Foundation of China (41930866, 41807012, 41671287), the Guangxi Natural Science Foundation (2018GXNSFGA281003, 2018GXNSFBA281136), the National Key Research and Development Program of China (No. 2016YFC0502403), and the Open Fund of Key Laboratory of Agro-ecological Processes in Subtropical Region, CAS (ISA2015301). Zhiyong Fu acknowledges funding from the Young Scholars in Western China and the Youth Innovation Promotion Association of CAS. The authors thank Prof. Corrado Corradini and two anonymous reviewers for their valuable and constructive comments.

References

Ameli, A., Craig, J., McDonnell, J., 2015. Are all runoff processes the same? numerical experiments comparing a darcy-richards solver to an overland flow-based approach for subsurface storm runoff simulation. Water Resour. Res. 51, 10008–10028.
Berthelin, R., Hartmann, A., 2020. The shallow subsurface of karst systems: review and directions. In: Eurokarst 2018, Besançon. Springer. pp. 61–68.
Buttle, J.M., 2005. Isotope hydrograph separation of runoff sources. Encyclopedia Hydrol. Sci.
Chaplot, V., Bissonnais, Y.L., 2003. Runoff features for interrill erosion at different rainfall intensities, slope lengths, and gradients in an agricultural loessial hillslope. Soil Sci. Soc. Am. J. 67, 844–851.
Chen, H., Liu, J., Wang, K., Zhang, W., 2011. Spatial distribution of rock fragments on steep hillslopes in karst region of northwest guangxi, china. Catena 84, 21–28.
Chen, H., Wang, K., 2004. Characteristics of karst drought and its countermeasures. Res. Agric. Modernization 25, 70–73.
Chen, H., Yang, J., Fu, W., He, F., Wang, K., 2012. Characteristics of slope runoff and sediment yield on karst hill-slope with different land-use types in northwest guangxi. Trans. Chin. Soc. Agric. Eng. 28, 121–126.
Du, E., Jackson, C.R., Klaus, J., McDonnell, J.J., Griffiths, N.A., Williamson, M.F., Greco, J.L., Bitew, M., 2016. Interflow dynamics on a low relief forested hillslope: lots of fill, little spill. J. Hydrol. 534, 648–658.
Dunne, T., Zhang, W., Aubry, B.F., 1991. Effects of rainfall, vegetation, and micro-topography on infiltration and runoff. Water Resour. Res. 27, 2271–2285.
Fan, Y., Clark, M., Lawrence, D.M., Swenson, S., Band, L., Brantley, S.L., Brooks, P., Dietrich, W.E., Flores, A., Grant, G., et al., 2019. Hillslope hydrology in global change research and earth system modeling. Water Resour. Res. 55, 1737–1772.
Fleury, P., Maréchal, J.C., Ladouche, B., 2013. Karst flash-flood forecasting in the city of nı̂mes (southern France). Eng. Geol. 164, 26–35.
Freer, J., McDonnell, J.J., Beven, K., Peters, N.E., Burns, D.A., Hooper, R., Aulenbach, B., Kendall, C., 2002. The role of bedrock topography on subsurface storm flow. Water Resour. Res. 38.
Fu, T., Chen, H., Wang, K., 2015a. Structure and water storage capacity of a small karst aquifer based on stream discharge in southwest china. J. Hydrol. 534, 50–62.
Fu, T., Chen, H., Zhang, W., Nie, Y., Gao, P., Wang, K., 2015b. Spatial variability of surface soil saturated hydraulic conductivity in a small karst catchment of southwest china. Environ. Earth Sci. 74, 2381–2391.
Fu, Z., Chen, H., Xu, Q., Jia, J., Wang, S., Wang, K., 2015c. Role of epikarst in near-surface hydrological processes in a soil mantled subtropical dolomite karst slope: implications of field rainfall simulation experiments. Hydrol. Process. 30, 795–811.
Fu, Z., Chen, H., Zhang, W., Xu, Q., Wang, S., Wang, K., 2015d. Subsurface flow in a soil-mantled subtropical dolomite karst slope: a field rainfall simulation study. Geomorphology 250, 1–14.
Gan, Y., Dai, Q., Fu, W., Yan, Y., Peng, X., 2016. Characteristics of soil erosion on karst slopes under artificial rainfall experiment conditions. Chin. J. Appl. Ecol. 27, 2754–2760.
Graham, C.B., Woods, R.A., Mcdonnell, J.J., Lin, H., Flühler, H., Otten, W., Vogel, H.J., 2010. Hillslope threshold response to rainfall: (1) a field based forensic approach. J. Hydrol. 393, 65–76.
Guo, L., Chen, J., Lin, H., 2014. Subsurface lateral preferential flow network revealed by time-lapse ground-penetrating radar in a hillslope. Water Resour. Res. 50, 9127–9147.
Hartmann, A., Gleeson, T., Wada, Y., Wagener, T., 2017. Enhanced groundwater recharge rates and altered recharge sensitivity to climate variability through subsurface heterogeneity. Proc. Natl. Acad. Sci. U.S.A. 114, 2842.
Hartmann, A., Goldscheider, N., Wagener, T., Lange, J., Weiler, M., 2014. Karst water resources in a changing world: review of hydrological modeling approaches. Rev. Geophys. 52, 218–242.
Hu, K., Chen, H., Nie, Y., Wang, K., 2015. Seasonal recharge and mean residence times of soil and epikarst water in a small karst catchment of southwest china. Scientific Rep. 5, 10215.
Jiang, Z., Lian, Y., Qin, X., 2014. Rocky desertification in southwest china: impacts, causes, and restoration. Earth Sci. Rev. 132, 1–12.
Leh, M.D., Chaubey, I., Murdoch, J., Brahana, J.V., Haggard, B.E., 2008. Delineating runoff processes and critical runoff source areas in a pasture hillslope of the ozark highlands. Hydrol. Process. 22, 4190–4204.
Li, X.Y., Contreras, S., Solé-Benet, A., Cantón, Y., Domingo, F., Lázaro, R., Lin, H., Wesemael, B.V., Puigdefábregas, J., 2011. Controls of infiltration-runoff processes in mediterranean karst rangelands in se spain. CATENA 86, 98–109. https://doi.org/10.1016/j.catena.2011.03.003.. URL:http://www.sciencedirect.com/science/article/pii/S0341816211000555.
Liu, M., Xu, X., Sun, A.Y., Wang, K., Liu, W., Zhang, X., 2014. Is southwestern china experiencing more frequent precipitation extremes? Environ. Res. Lett. 9, 064002.
McDonnell, J.J., 2003. Where does water go when it rains? moving beyond the variable source area concept of rainfall-runoff response. Hydrol. Process. 17, 1869–1875. https://doi.org/10.1002/hyp.5132.
Tromp-van Meerveld, H., McDonnell, J., 2006a. Threshold relations in subsurface stormflow: 1. a 147-storm analysis of the panola hillslope. Water Resour. Res. 42.
Tromp-van Meerveld, H., McDonnell, J., 2006b. Threshold relations in subsurface stormflow: 2. The fill and spill hypothesis. Water Resour. Res. 42.
Peng, T., Wang, S., 2012. Effects of land use, land cover and rainfall regimes on the surface runoff and soil loss on karst slopes in southwest china. Catena 90, 53–62.
Peng, X., Dai, Q., Ding, G., Li, C., 2019. Role of underground leakage in soil, water and nutrient loss from a rock-mantled slope in the karst rocky desertification area. J. Hydrol. 578, 124086. https://doi.org/10.1016/j.jhydrol.2019.124086.

Peng, X., Dai, Q., Li, C., Yuan, Y., Zhao, L., 2017. Effect of simulated rainfall intensities and underground pore fissure degrees on soil nutrient loss from slope farmlands in karst region. Trans. Chin. Soc. Agric. Eng. 33, 131–140.

Qin, L., Bai, X., Wang, S., Zhou, D., Li, Y., Peng, T., Tian, Y., Luo, G., 2015. Major problems and solutions on surface water resource utilisation in karst mountainous areas. Agric. Water Manag. 159, 55–65.

Wang, S., Chen, H.S., Fu, Z., Wang, K., 2016. Temporal stability analysis of surface soil water content on two karst hillslopes in southwest china. Environ. Sci. Pollut. Res. 23, 25267–25279.

Weiler, M., McDonnell, J.J., Tromp-van Meerveld, I., Uchida, T., 2005. Subsurface stormflow. Encyclopedia Hydrol. Sci.

Wang, S., Chen, H., Fu, Z., Wang, K., 2017. Evaluation of the spatial pattern of surface soil water content of a karst hillslope in southwest china using a state-space approach. Arch. Agron. Soil Sci. 1800–1813. https://doi.org/10.1080/03650340.2017.1307507.

Wilcox, B.P., Taucer, P.I., Munster, C.L., Owens, M.K., Mohanty, B.P., Sorenson, J.R., Bazan, R., 2008. Subsurface stormflow is important in semiarid karst shrublands. Geophys. Res. Lett. 35.

Yang, J., Nie, Y., Chen, H., Wang, S., Wang, K., 2016. Hydraulic properties of karst fractures filled with soils and regolith materials: Implication for their ecohydrological functions. Geoderma 276, 93–101.

Yuan, D., 1994. Chinese Karstology. Geology Press, Beijing.

Zhao, Q., Li, D., Zhuo, M., Guo, T., Liao, Y., Xie, Z., 2015. Effects of rainfall intensity and slope gradient on erosion characteristics of the red soil slope. Stochastic Environ. Res. Risk Assess. 29, 609–621.

Zhao, X., Huang, J., Gao, X., Wu, P., Wang, J., 2014. Runoff features of pasture and crop slopes at different rainfall intensities, antecedent moisture contents and gradients on the chinese loess plateau: A solution of rainfall simulation experiments. Catena 119, 90–96.

Zhu, X., Chen, H., Fu, Z., Wang, K., 2017. Runoff and nitrogen loss characteristics in soil-epikarst system on a karst shrub hillslope. Chin. J. Appl. Ecol. 28, 2197–2206.